Zooplankton-microplastic exposure in Delaware coastal waters: Atlantic blue crab (*Callinectes sapidus*) larvae case study

Todd X. Thoman [a,*], Tobias Kukulka [a], Jonathan H. Cohen [b], Hayden Boettcher [b]

[a] *School of Marine Science and Policy, University of Delaware, 272 The Green, Newark 19716, DE, USA*
[b] *School of Marine Science and Policy, University of Delaware, 700 Pilottown Rd, Lewes 19958, DE, USA*

ARTICLE INFO

ABSTRACT

High microplastic concentrations in the Delaware Bay have prompted concern regarding harm to local species. We consider the extent to which the zooplankton is exposed to bay-derived microplastics, focusing on Atlantic blue crabs (*Callinectes sapidus*) during offshore larval migration. We simulate regional flow fields for a spawning season in the Delaware coastal system to advect passive Lagrangian microplastic and zooplankton tracers. Microplastic exposure levels are estimated from tracer distributions. Field sampling of zooplankton and microplastic concentrations for the Delaware Bay mouth and the adjacent shelf in August 2020 is utilized to appraise model performance. Three mechanisms elevating microplastics exposure are identified: zooplankton transport into microplastic-laden tidelines, displacement of microplastics into the buoyant outflow current, and aggregation in offshore plume fronts. Organization via the above mechanisms substantially enhance microplastic exposures over zooplankton migrations (by an average factor of at least 3.8).

1. Introduction

Over the past few decades, expanding usage, inefficient disposal, and long decomposition times have turned plastics into a growing pollution concern (Hale et al., 2020). Manufactured on a broad range of scales, use and environmental degradation breaks these materials down to smaller and smaller sizes. Once passing under five millimeters in diameter, these materials are referred to as microplastics, a form which has dispersed across the globe (Hale et al., 2020). Marine microplastics are under intense scrutiny as oceans collect, sort, and retain terrigenous inputs (Cohen et al., 2019; Hale et al., 2020; Kukulka and Brunner, 2015; López et al., 2021; Mason et al., 2022). Although the impacts of these pollutants on organisms are still not fully understood, the potential for adverse health effects is a critical topic of ongoing research (Cole et al., 2015; Gambardella et al., 2017; Hale et al., 2020). The first step of this research is determining where microplastics occur in the global oceans and where they accumulate, using numerical and observational techniques jointly to derive key insights (Bikker et al., 2020; Cohen et al., 2019; Kukulka and Brunner, 2015; López et al., 2021). Recent sampling efforts have revealed high levels of microplastic pollution in the Delaware Bay, an estuary located in the Mid-Atlantic Bight between Delaware and New Jersey, USA (Cohen et al., 2019). Cohen et al. (2019)

report microplastic concentrations on the scale of 0.7 pieces/m^3 seemingly stemming predominantly from source tributaries (2–3 pieces/m^3); however, reported models indicate potential hotspots in the shape of long, branching, along-estuary bands (a.k.a. tidelines) stretching the length of the bay that may possess concentrations orders of magnitude greater than those reported at selected stations. These high microplastic concentrations, which exceed those in nearby open oceans by over an order of magnitude (Kukulka and Brunner, 2015), raise concerns for potential harm to local ecosystems. In this work, we take the next step in considering the impact of microplastics on zooplankton communities upon export to the Delaware shelf region. More specifically, we aim here to categorize the pathways that lead to exposure of zooplankton to microplastics, as well as to estimate the resultant exposure to this pollutant using a commercially-important case study - Atlantic blue crab (*Callinectes sapidus*) larvae.

To the authors' knowledge, *C. sapidus* has yet to be directly studied for interactions with microplastics. However, ingestion of these pollutants has been observed in varied zooplankton species (Cole et al., 2015; Cole et al., 2013; Gambardella et al., 2017; Setälä et al., 2014; Sun et al., 2017). Amongst these species are numerous crustaceans, such as brine shrimp (Cole et al., 2013; Gambardella et al., 2017), copepods (Cole et al., 2015; Cole et al., 2013; Setälä et al., 2014), and zoeae and

megalopae of Brachyuran crabs (Cole et al., 2013). While laboratory studies rarely revealed significant mortality effects stemming from ingestion (Cole et al., 2013; Gambardella et al., 2017), reduced fecundity (Cole et al., 2015), reduced swim speed (Gambardella et al., 2017), and altered feeding behaviors (Cole et al., 2015) have been observed, signaling worsened health amongst zooplankton populations potentially caused by physical harm/obstruction (Hale et al., 2020) or toxicity from chemical leaching (Talsness et al., 2009). In order to determine the overall risk of these impacts, both the response to pollutant and the exposure to the pollutant are required. While a full study of biological impacts of exposure are beyond the scope of the current work, exposure regions and concentrations will be considered here.

C. sapidus possesses a larval life history that has been the subject of considerable research over the past couple decades. While benthic adults of this species reside within home estuaries along the eastern North American coastline, spawning females migrate to the estuary mouth to release pelagic larvae on ebbing nighttime tides (Epifanio, 2019; Epifanio and Garvine, 2001; Tankersley et al., 1998). Study of the larval transport and recruitment phenomenon has painted the image of a multi-step passive migration for zoea and megalopa larval stages. Epifanio and Garvine (2001) suggested that larval transport consists of three phases: (1) larval export and southward transport within river-derived freshwater outflow to the coastal ocean, (2) counter-transport north via offshore currents driven by coastal upwelling-favorable winds, and (3) periodic reintroduction of larvae back into the natal estuary during downwelling-favorable wind events later in the spawning season. This anticipated larval transport loop represents a practical concern in regards to exposure to microplastics. If larvae are anticipated to follow offshore migration loops, continued export of microplastics from the Delaware Bay may accumulate within larval patches over time through the recirculation patterns necessary for successful larval settlement. Particularly in early larval stages, *C. sapidus* transport via surface currents, as larvae preferentially remain within the upper one to two meters of the water column at all times of day (McConaugha et al., 1983; Provenzano et al., 1983). As largely passive tracers, one may anticipate that both the larvae and buoyant plastics will follow similar pathways upon export from the bay, preserving microplastic exposure over time apart from gradual diffusive processes (i.e. turbulence and submesoscale eddies) or encounters with regional-scale convergent flow structures (i.e. coastal plume fronts (Tilburg et al., 2009)). For these reasons, *C. sapidus* appears to provide an important case study into the presence and underlying mechanisms for coastal microplastic exposure.

Overall, the larval migration predictions of Epifanio and Garvine (2001) have withstood study and challenge [for example, Biermann et al., 2016] for over two decades; however, the authors' overview is fairly idealized. Subsequent numerical work has clarified the larval recruitment behavior to define three distinct migration pathways (Tilburg et al., 2005). In the first migration pathway (hereafter referred to as tidal-trapping), larvae do not leave the bay. Instead, larvae become trapped on the northern end of the bay mouth, where, in the absence of strong winds, flow is primarily oscillatory and driven by the tides. The second path (hereafter referred to as the bouyant plume loop) involves downwelling winds upon flushing from the bay retaining larvae near the Delaware coast, where persistent upwelling winds return larvae directly through the buoyant coastal current. The third follows closely the proposed pathway of Epifanio and Garvine (2001); this path (hereafter referred to as the offshore wind loop) sees coastal upwelling-favorable winds on export from the bay causing the larvae to transit to the northeast, and re-entering the bay via subsequent downwelling wind events. Over several simulated months, Tilburg et al. (2005) found that the third pathway served as the predominant course of successful larval migrations, representing approximately 60 % of larvae returned to the bay.

The flow dynamics of the Delaware Bay introduce an additional degree of complexity to the exposure problem - larvae and microplastics may be spatially separated prior to export from the estuary. Microplastic

tracer models of the Delaware Bay indicate a preference for collection near the centerline of the bay, near or overlying the thalweg and bordering the river-derived outflow (Cohen et al., 2019). This tendency could be tied to bathymetry-driven coherent convergent flow in estuaries with deep central channels, such as axial convergence (Nunes and Simpson, 1985) or Lagrangian residual circulation (Kukulka and Chant, 2022). Whatever the driving mechanism of the microplastic arrangement in the Delaware Bay, the organization of microplastics by estuarine dynamics may be expected to control the early onset exposure of larvae to this pollutant, as hatching and release of *C. sapidus* larvae, for example, is not anticipated to be limited to these narrow tidelines (Ogburn and Habegger, 2015). In order to understand the potential for interaction with and risk to larvae from microplastics, one must then ask if and how coastal flow bring larvae and microplastics-laden waters together.

In this study, we utilized a regional hydrodynamic model of the Delaware Bay and surrounding coastal ocean to simulate realistic flow conditions. Resulting flow fields were utilized to drive Lagrangian tracer fields representing *C. sapidus* larvae and microplastics from distinct source locations. Tracer transport and distributions were modeled and compared to field observations of surface microplastics and *C. sapidus* larval concentrations collected outside the mouth of the Delaware Bay from August 18–20, 2020 to assess model behavior. Modeled tracer paths were studied against environmental conditions to determine the pathways of microplastic exposure, the necessary environmental conditions for enhanced exposure, and the magnitude of exposure. Insights into coastal microplastic exposure in the current study provide context for future questions of ecological risk to this commercially-important species, amongst other surface-advected coastal zooplankton species.

2. Methods

2.1. Delaware Bay regional model

A three-dimensional model of the Delaware Bay and the surrounding shelf waters constructed in the Regional Ocean Modeling System (ROMS) is utilized following the approach of Kukulka et al. (2017) and Cohen et al. (2019). This ROMS model incorporates realistic bathymetry and coastal geometry and solves the three-dimensional momentum and salinity fields within a terrain-following, curvilinear grid that admits sea surface height responses by tides and coastal upwelling/downwelling (Shchepetkin and McWilliams, 2005; Song and Haidvogel, 1994). The domain and construction of the grid utilized for this study is designed to match that of the previous Delaware Bay regional model designed by Whitney and Garvine (2006). Model horizontal resolutions are as fine as 750 m near the head of the Delaware Bay to admit higher resolution of complex flow in the narrow channel, but relax to up to eight km near the offshore edge of the coastal shelf for computational efficiency (Whitney and Garvine, 2006). The vertical dimension is in an s-coordinate system with ten vertical levels and coarser resolution away from the air-sea interface.

In line with the realistic structure of the domain, the model was driven by realistic environmental forcings. Surface winds were applied as a surface stress according to data from NOAA buoy 44009 (https://www.ndbc.noaa.gov/) located outside the mouth of the Delaware Bay. Winds were treated as horizontally homogeneous over the domain. Gaps in the time series were filled with data collected at station LWSD1, located at Lewes, DE, scaled to match winds proximate to buoy 44009 (Castellano and Kirby, 2011). As in the reference model of Whitney and Garvine (2006), river discharge was localized at the head of the Delaware Bay with outflow scaled to match the anticipated inflow of all collective tributaries. Raw data for river outflow were retrieved from the United States Geological Survey station at Trenton, NJ (site 01463500) (https://waterdata.usgs.gov/). Finally, realistic tides were constructed via the ADCIRC tidal database using nine tidal constituents. Of the nine, the M2 tidal constituent dominates tides in this region (Whitney and

Garvine, 2006) and the model presented here, while the overall tides present as semi-diurnal. This Delaware Bay ROMS model has been previously employed and tested for accuracy (Kukulka et al., 2017). In the current study, the regional model was run from September 2019 through October 2020 with the target study time being the spawning and larval development window of *C. sapidus* - May to September 2020. Model runs were performed with an internal time resolution of 150 s and outputs were saved for analysis with a temporal resolution of 1 h. Additional runs (not presented here) have been performed for 2008, 2009, and 2010 spawning seasons, yielding similar results.

2.2. Larval and microplastic Lagrangian tracers

To capture the transport of zooplankton and microplastics, we made use of a Lagrangian particle advection framework, following the technique of Mason et al. (2022) to employ inverse-distance-based weighting to fit the curvilinear model design. Tracers were advected with a five-minute time step. To define properties and distribution of the zooplankton, we further define these tracers as larval *C. sapidus*. Early stage *C. sapidus* larvae largely remain in the surface one to two meters of the water column (Epifanio, 2019; McConaugha et al., 1983; Provenzano et al., 1983) independent of any diel migration (Provenzano et al., 1983). It should be noted that late stage larvae, such as megalopae, may begin to migrate deeper into the water column (Biermann et al., 2016); however, in the present study, the vast majority of tracers either collect within the bay or transport far from the bay mouth by three weeks, an early estimate for when a zoea will molt into a megalopa (Costlow and Bookhout, 1959). Due to this behavior, as in Mason et al. (2022), tracers were considered "surface-trapped" such that horizontal velocities were taken from the surface-most grid layer and the vertical velocity was ignored. The approach is admissible for microplastics exported from Delaware Bay as these particles will predominantly be those that are positively buoyant (López et al., 2021).

Unlike Mason et al. (2022), this study employed targeted tracer releases to reflect observed microplastic input locations and larval spawning grounds. Tracers were released at three distinct locations (Fig. 1b). Tracers released at the head of the Delaware Bay (a) and off the coast of Bowers Beach, DE (b) represent microplastic delivery through the Delaware River and St. Jones/Murderkill Rivers, respectively. Tracers released at the mouth of the Delaware Bay towards the Delaware coastline (c) represent hatching locations of *C. sapidus*. Microplastic release locations were motivated by findings from Cohen et al. (2019), which shows high microplastics near these tributaries in field observations. Hatching locations were motivated by *C. sapidus* spawning behaviors, which are characterized by spawning at the mouth of natal estuaries (Epifanio, 2019; Epifanio and Garvine, 2001; Ogburn and Habegger, 2015), and targeted towards recovery of the larval migration loops. Although spawning may occur further onto the shelf as evidenced by observed tidal stream transport migrations associated with the timing of spawning events (Tankersley et al., 1998), our release locations match those of Tilburg et al. (2005) allowing us to compare our larval transport paths against existing studies. Likely, the most direct consequence of any discrepancy in spawning location is an increased capacity of larvae to be retained within the Delaware Bay mouth; however, the study by Tilburg et al. (2005) indicates that extended retention within the bay is overall less common than coastal transport pathways, a finding that is similarly observed in the current study.

Lagrangian "microplastic" tracers were released in the model beginning on May 1, 2020 with 20 tracers per release location. Subsequent tracers were released every two days. The release spacing created a relatively continuous trail of microplastics under most conditions aided by a multi-week residence time in the Delaware Bay. "Larval" tracers began releasing 60 days after the first "microplastic" releases to ensure that the microplastics had circulated throughout the bay and onto the shelf. Larval releases included 225 tracers per release and recurred weekly.

Resulting tracer field concentrations were scaled to realistic levels for analysis based upon previously reported field observations.
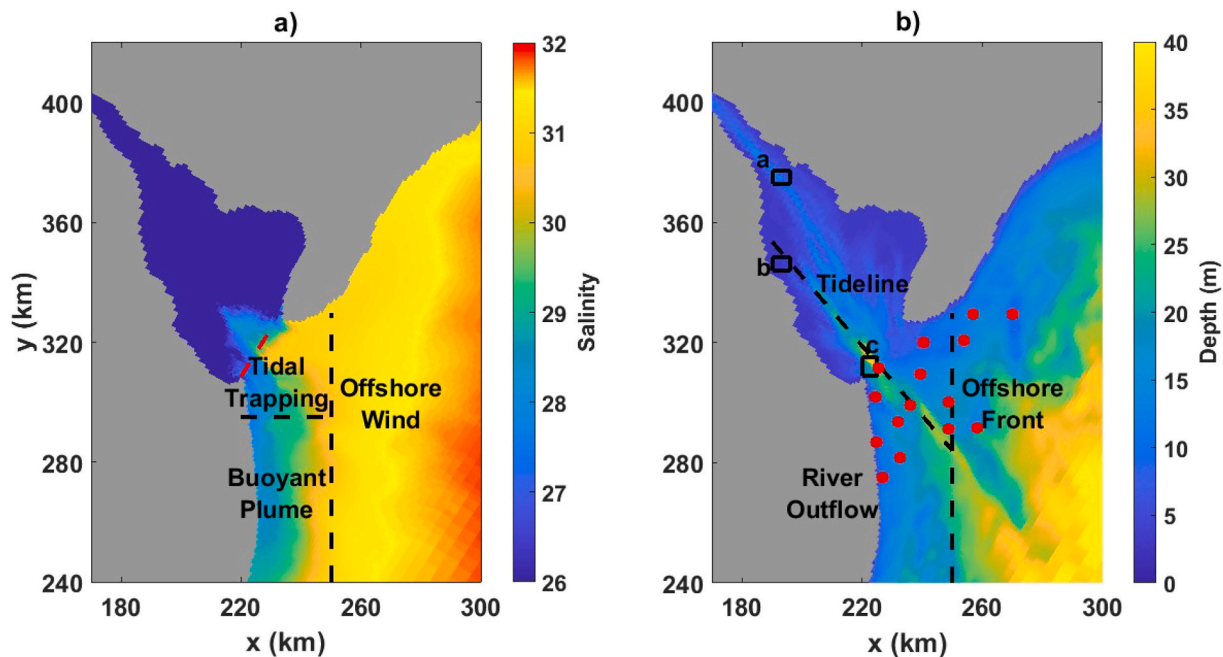

Fig. 1. (a) Map of spatial delineations used to determine larval return and larval migration pathways. The red dashed line indicates the threshold for particles to be "returned" to the bay for subsequent settlement, while the black dashed lines indicate thresholds for division into the Offshore Wind Loop, Buoyant Plume Loop, and Tidal Trapping migration pathways. Salinity is used to show position of the coastal current under limited winds. (b) Map of spatial delineations for the occurrence of three principle exposure mechanisms: tideline-assisted exposure, exposure in river outflow, and aggregation in the offshore plume front. Bathymetry is shown to underscore the thalweg as a critical reference point. Tracer release locations (boxes a–c) and stations for observational sampling (red dots) are marked. (For interpretation of the references to colour in this figure legend, the reader is referred to the web version of this article.)

Callinectes sapidus larvae were scaled based upon a measured zoea larval patch found in the coastal current roughly ten kilometers south of the Delaware Bay on August 10, 1998 (Natunewicz and Epifanio, 2001). These observations show mean concentrations of approximately 200 larvae/m^3. Scaling by average dimensions of patches observed from July to September 1998 suggests approximately 6.2×10^8 zoeae spawned into the observed larval patch. This calculation followed the assumption that zoeae will be within the upper meter of the water column (Epifanio, 2019; McConaugha et al., 1983; Provenzano et al., 1983). Therefore, we took our larval releases to represent 6.2×10^8 individuals split evenly amongst the larval tracers, such that each tracer represented 1,386,700 larvae. Scalings remained constant over the runs and neglected morbidity and mortality during analysis. Associated error does not influence results, as exposure concentrations are a function of microplastic concentrations and independent of the exact larval count. The microplastic concentrations of Cohen et al. (2019) taken near the source tributary locations modeled here show microplastic concentrations of approximately 2.5 pieces/m^3. These concentrations were multiplied by the surface area of release locations (a) and (b) (Fig. 1b) to estimate the number of microplastics in the upper meter of the water column per release. Division by the number of tracers per release set the scaling as 2,995,200 microplastics per tracer.

Microplastic concentrations were binned and assigned to a grid with 2 km-by-2 km cell dimensions. Exposure estimates were determined via a multi-step analysis. First, tracer paths were filtered to only those that returned to the bay to allow for settlement. Return was determined by being up-bay of the threshold between Cape May, NJ and Cape Henlopen, DE (Fig. 1a, red line) between three to five weeks after spawning, consistent with expected viability windows for larval settlement (Costlow and Bookhout, 1959; Epifanio, 2019) and prior modeling efforts (Tilburg et al., 2005). Timing of larval settlement is controlled by physical conditions, such as temperature through altering duration of intermolt periods (Costlow and Bookhout, 1959) and chemical cues from the estuarine environment that initiate settlement (Epifanio and Cohen, 2016). Such complexity results in a wide range of viable settlement timings; however, the intricacies controlling such timings is beyond the scope of the current work and the regional model herein, encouraging the use of a timed return to the bay over a distinct settlement process as the "end" of larval transport. Of the larval tracers that return to the bay, their paths prior to return were used to divide the population into three migration pathways similar to Tilburg et al. (2005) for comparison of exposure between the three distinct migrations. The three divisions can be seen in Fig. 1a with black dashed lines dividing the three spatially. If a particle passed east of the $x=250$ km line, the particle was considered to take the Offshore Wind Loop. Else, if the particle did not pass $x=250$ km, but moved below the $y=295$ km line, the particle was assigned the Buoyant Plume Loop. Any remaining particles were assigned to Tidal Trapping.

For each returned particle, a time series of microplastic exposure concentrations was generated by interpolating the microplastic concentration field locally to the particle via bilinear interpolation. Results presented in Section 3.4.4 represent the averaged instantaneous exposures of tracers as a function of time since spawning, as well as a time series of net exposure taken as the time integral of mean instantaneous exposure since spawning. Principal exposure mechanisms (defined below in Section 3.4) were also categorized according to the location of the tracer when instantaneous exposure first exceeded 4 microplastic pieces/m^2. (Note: From here forwards, pieces/m^2 is utilized over pieces/m^3 to better conform to model output of a surface-trapped tracer, with the understanding that our assumption of larvae being retained to the surface meter of the water column (McConaugha et al., 1983; Provenzano et al., 1983) allows for a one-to-one transformation between units.) This threshold value was determined empirically to be representative of exposure levels distinctly formed via key aggregation zones within each of the three exposure pathways observed in the model. The

spatial divisions are shown in Fig. 1b.

2.3. Field observations of C. sapidus larvae and microplastics

While the modeling techniques above provide convenient and thorough insight into the movement of larvae and microplastics within prescribed conditions, it is important to highlight consistencies between any numerical approach and the natural system. While sampling efforts for microplastics have been undertaken within the Delaware Bay (Cohen et al., 2019), reported samples end at the bay mouth, rather than extending onto the shelf. Further, larval observations tend to be limited in scope, targeting either a single station or line over time (Biermann et al., 2016) or tracking a particular feature (Natunewicz and Epifanio, 2001). In order to back the modeling efforts and verify dynamics and distributions of larvae and microplastics on the shelf, additional sampling efforts were undertaken on August 18–20, 2020 in order to provide baseline insights for comparison to model results. The sampling effort consisted of fifteen stations extending from the mouth of the Delaware Bay along the New Jersey coast, along the Delaware coast, and across the shelf (Fig. 1b). Each station was sampled once during this multi-day cruise effort. The exception is the station northeast of Cape Henlopen, DE, which was sampled on all three days and has averaged results presented below. A CTD profile was first recorded upon arrival to each station (SeaBird SBE19 CTD). Following retrieval of the CTD, a tucker trawl was deployed with a nylon mesh with mesh size of 100 µm. The net was towed at the surface for approximately 5 min at 2 knots. The volume of water sampled is computed according to the area of the mouth of the net (0.25 m^2) multiplied by the distance traveled determined via an attached flow meter (General Oceanics).

Contents from each net tow were separated into two pre-cleaned glass jars and immediately preserved in 4 % buffered formaldehyde. One-fifth of the sample was analyzed for larvae and the remainder for microplastics. *Callinectes sapidus* larvae were identified and enumerated underneath a stereomicroscope. For larval identification, we followed Dittel and Epifanio (1982), utilizing morphological characteristics of larvae/post-larvae for species in the study region as presented in Sandifer (1972) and Bullard (2003), and in original descriptions as available. For microplastics, collected samples were digested with potassium hydroxide to break down organic matter (Rochman et al., 2015). The digested samples were subjected to density separation twice, first using a solution of sodium chloride and again using a solution of sodium iodide (Quinn et al., 2017). All suspected microplastics were isolated onto a low-e glass slide under a stereomicroscope. All particles were subsequently analyzed via microscopic Fourier-transform infrared (µFTIR) spectroscopy to confirm the chemical composition of each microplastic particle. In total, 809 particles were analyzed, an average of 42.2 ± 24.7 particles per station. Out of the total suspected particles, 589 (72.8 %) were confirmed as microplastics based on spectral comparison against a custom library. Counts of larvae and microplastics are scaled up to represent accurate quantities for the full volume of the collected samples, and concentrations are computed accordingly. Preventative measures were employed to mitigate plastic contamination during analysis. All tools and equipment were composed of glass or stainless steel and neon-orange cotton jumpsuits were worn to prevent contamination from clothing. Samples were kept covered when not in use and all sorting was performed under a laminar flow hood. Photographs of the suspected microplastics were taken immediately following sorting and a unique particle ID given to each piece. All particles found on the slide during µFTIR analysis that were not in the original image were ignored as contaminants.

2.4. Wind and river discharge during 2020 spawning season

Here, we review the prevailing environmental forcings controlling this system during the 2020 model and corresponding field sampling campaign. Prevailing wind conditions for late Spring to early Fall 2020

display similar patterns to earlier observed years. During May, wind orientation shows rapid inversions from coastal upwelling-favorable to coastal downwelling-favorable with periods ranging from several hours to a couple days (Fig. 2b). During this same window, winds tend to favor an overall westerly orientation. During June and July, southwesterly winds are by far most prevalent, indicating a predisposition for coastal upwelling during these months (Fig. 2b). In late August to September, winds begin to shift, taking on the periodic intensely downwelling-favorable northeasterly orientations (Fig. 2b). While June and July winds appear largely unfavorable to larval return due to minimal downwelling winds, periodic intense downwelling winds in May and September appear conducive to anticipated return of *C. sapidus* larvae to the Delaware Bay (Biermann et al., 2016; Epifanio, 2019; Epifanio and Garvine, 2001; Tilburg et al., 2005). This potential for larval return highlights 2020 as a meaningful year for this study, as exposure without larval return has no effect on the overall health of the fishery.

Through much of the potential spawning window, freshwater discharge remains steadily between 200 and 400 m³/s. Three large storm events are captured in the freshwater forcing: one in mid-April, one in early May, and one at the beginning of August, with freshwater effects being observed at the mouth two weeks following the passage of the storm (Fig. 2c). Although infrequent, storm events may enhance flushing of particles from the bay, even when particles organize north of the river outflow current (Mason et al., 2022).

While tides function as the third forcing of the hydrodynamic model and play important roles in enhancing in-bay organization of particles (Kukulka and Chant, 2022; Mason et al., 2022; Nunes and Simpson, 1985), sensitivity tests show particle organization for both spring and neap tidal phases, and winds dominate coastal particle transport. As such, discussion of the tides will be limited within this work.

3. Results and discussion

3.1. Larval transport and return

Larval transport pathways were analyzed for May through August 2020. Three distinct pathways for successful return or retention of

C. sapidus larvae were observed, correlating to those presented in the previous literature (Tilburg et al., 2005). These include the tidally-trapped particles oscillating within the northern waters of the bay mouth, where tracers collect within a high-density patch moved by tidal flooding and ebbing (Fig. 3a). Tidal trapping occurs via early onset upwelling-favorable winds, such that larval release/spawning is met with transport to the north of the thalweg, where tidally-averaged currents are weak, followed by weak winds or winds with rapidly varying orientations. The second observed migration pathway is the buoyant plume loop (Fig. 3b), in which larvae are exported within the river plume and follow the coastal current south in the presence of downwelling winds. Upwelling-favorable winds reverse surface transport direction, returning larvae to the estuary. The final observed migration pathway is the offshore wind loop (Fig. 3c), in which tracers experience upwelling-favorable winds while flushing from the estuary. These conditions push larvae northeast and downwelling wind pulses return larvae to the bay. While the former two pathways most often result in successful return to the bay by three weeks, the offshore wind loop can take anywhere from three to five weeks. As in Tilburg et al. (2005), the offshore loop occurred most frequently, showing for 11.0 % of larvae as opposed to 1.6 % of larvae retained in tidal-trapping and 0.3 % returned by the buoyant plume loop. Compared to Tilburg et al. (2005) in which the offshore wind loop was reported to account for just over 60 % of successful larval returns, this pathway accounts for 85.4 % of returns in our simulations for 2020, while tidal-trapping and the buoyant plume loop account for 12.4 % and 2.2 % of returned larvae, respectively.

3.2. Microplastic tracer distributions

Simulated microplastic distributions are predominantly shaped by the winds, taking on one of three distinct patterns depending upon wind orientations (Fig. 4); river discharge and tides interact with winds to influence flushing of microplastics to the coastal ocean. In cases where winds are oriented cross-shelf (i.e. - roughly along-bay) or are overall weak (<5 m/s), microplastic tracers take the shape of thin, centrally-aligned tidelines within the Delaware Bay (Fig. 4a), as previously observed by Cohen et al. (2019) and Mason et al. (2022). This trend is
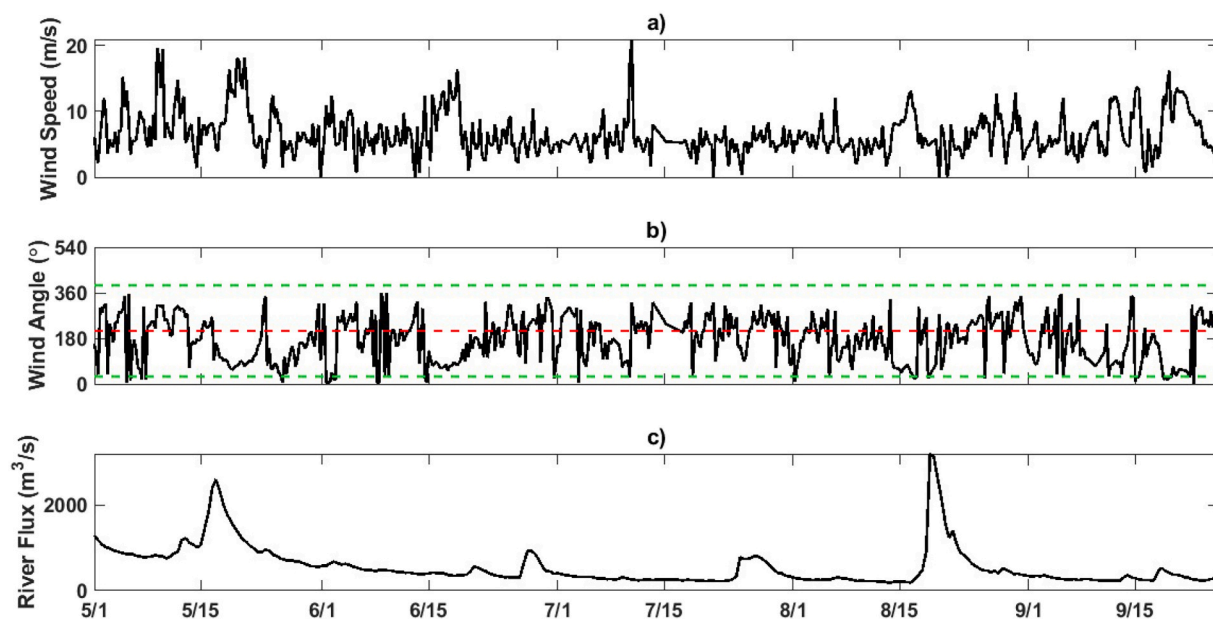
Fig. 2. (a) Wind speed, (b) wind orientation in meteorological standard, and (c) freshwater discharge for the 2020 larval spawning and transport window, May 1, 2020 to September 26, 2020. Dashed green lines in the wind orientation figure represent peak coastal alignment for downwelling winds, the red dashed line indicates the same for upwelling winds. The y-axis is extended to better visualize "wrap-around" for clarity of upwelling-favorable and downwelling-favorable orientations. Freshwater discharge is delayed by two weeks representing the transport time from the Delaware River tributary to the bay mouth. (For interpretation of the references to colour in this figure legend, the reader is referred to the web version of this article.)
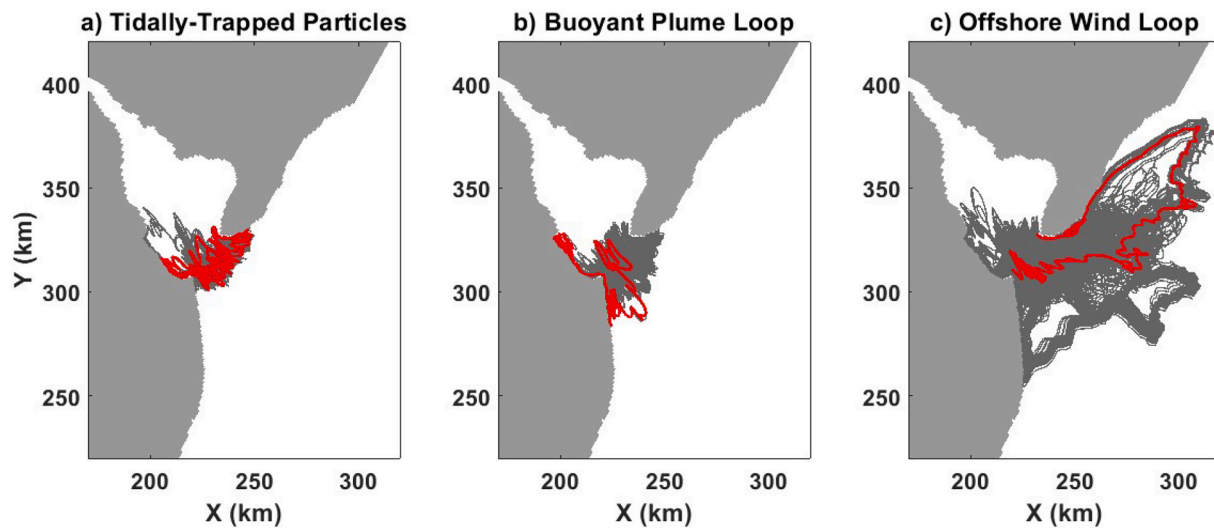
Fig. 3. Pathways for successful larval return to the bay divided into three classes. Pathways are labelled for comparison to those discussed in Section 1 from Tilburg et al. (2005). All successful paths are shown in grey and a selected example path is clarified in red. (For interpretation of the references to colour in this figure legend, the reader is referred to the web version of this article.)
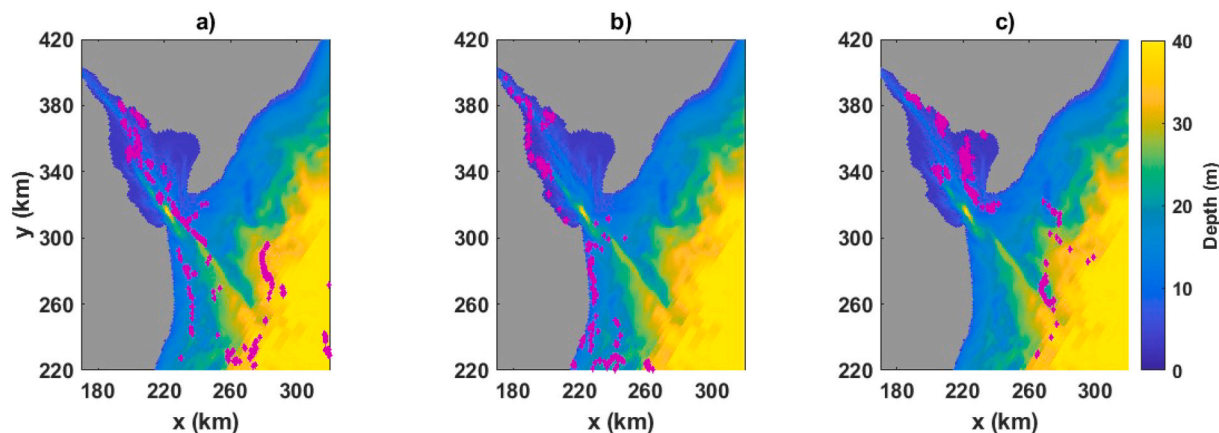

Fig. 4. Sample microplastic distributions generated during simulated windows with (a) winds oriented cross-shelf (i.e. - no coastal upwelling or downwelling winds), (b) coastal downwelling-favorable winds, and (c) coastal upwelling-favorable winds. The tracer fields overlie bathymetry for comparison with bathymetric channels.

observed for microplastics released from both the Delaware River and St. Jones/Murderkill river tributary locations, demonstrating a convergent transport along the length of the estuary. This convergence aligns well with the thalweg of the bay, supporting prior observations (Cohen et al., 2019) and assertions of either axial convergence (Nunes and Simpson, 1985) or Lagrangian residual convergence (Kukulka and Chant, 2022) of tracers via the frictional interactions of flood tides with bathymetric channels. Flushing tends to be weak (Mason et al., 2022), but gradual release is likely driven by interaction with the river outflow bordering the tideline to the south. When winds are oriented favorably for coastal downwelling or upwelling, microplastic tracers tend to break away from convergent regions over the thalweg (Fig. 4b, c). Downwelling winds shift particles towards the Delaware coast, while upwelling winds displace particles towards the New Jersey coast. If winds are intense or prolonged, this can result in compression of tracer patches along the coastline. Under migration via downwelling winds, tracers enter into the riverine outflow, leading to enhanced along-estuary transport and flushing onto the coast, a process accelerated under these conditions by high river discharge events and ebbing tides. During upwelling wind events, tracers migrate north to comparatively quiescent waters north of the Delaware River outflow. In this region, flushing occurs slowly in response to sustained upwelling winds. Within the bay,

tracers undergo secondary weaker aggregation in relation to shallower and smaller finger-like channels north of the thalweg (Fig. 4c). This secondary aggregation lends further credence to the role of bathymetrically-controlled convergent mechanisms in Delaware Bay (Kukulka and Chant, 2022; Nunes and Simpson, 1985).

After flushing onto the shelf, microplastic tracers organize cross-shelf primarily in response to along-shore winds (Lentz and Fewings, 2012) and convergence at the offshore plume front (Tilburg et al., 2009). When winds are weak, minimal cross-shelf motion occurs. Tracers exported along the central tideline predominantly follow the offshore edge of the river plume (Fig. 4a), while tracers exported within the plume will remain within the coastal current. Under downwelling winds, particles collect along the Delaware coastline while transporting south via the coastal current (Fig. 4b). Paired with anticipated narrowing and intensification of the coastal current during downwelling wind conditions (Fong and Geyer, 2001; Whitney and Garvine, 2005), tracers are rapidly transported away from the Delaware Bay. Under upwelling winds, particles may flush from the bay north of the river plume, leading to rapid cross-shelf loss from the system; particles in the coastal current are moved to the offshore plume front (Fig. 4c), which slows transport and accumulates material by acting as a semi-permeable barrier to surface tracers (Thomson et al., 2014; Tilburg et al., 2005). Tracers can be lost

from the coastal current through gradual drift through the plume front under sustained winds (Thomson et al., 2014).

3.3. Comparison to observed larval and microplastic distributions

Callinectes sapidus zoea larvae and near-surface microplastics were sampled in the Delaware Bay mouth and adjacent shelf waters from August 18–20, 2020. This sampling window was preceded by a period of upwelling-favorable winds, followed by downwelling-favorable winds during the sampling window. Downwelling winds lasted for roughly a day before returning to an upwelling orientation. During this time, a freshwater pulse from a preceding storm event near the beginning of August reached the mouth of the bay (Fig. 2).

Zoea larvae showed a patchy distribution on the shelf, reaching concentrations as high as 94 larvae/m³ at select stations following the plume front, tracking south with the coastal current and following north around Cape May, NJ (Fig. 5). Simulated larval tracers show similar qualitative patchiness and return reasonably consistent distributions in the coastal current and plume front resulting from repetitive wind inversions and high flushing through downwelling winds and high river discharge. Direct comparison, particularly to the north is hindered by limited spawning distribution in the model. Spawning events are reported as wide-spread, and spatially concurrent with coastal waters just beyond natal estuaries rather than with salinity distribution (Jivoff et al., 2017; Ogburn and Habegger, 2015; Tankersley et al., 1998). Discrepancy in the chosen finite spawning location in the model and variation in actual spawning locations utilized in the bay may be one reason behind more intense southern distribution of modeled larvae. For our purposes, our limited release distribution is deemed appropriate as it corresponds to existing larval transport studies (Tilburg et al., 2005) and additional northern spawning locations are anticipated to split behavior between trapping in tidelines and flushing north beyond our system.

We observe microplastics at all coastal sampling stations, ranging from 0.07 to 0.2 microplastic pieces/m³ (Fig. 6). An in-depth comparison to model data is not possible due again to limited data availability; to the best of the authors' knowledge, distributed microplastic samples in the Delaware coastal ocean have not been previously reported. Qualitatively, model distributions of microplastics display strong agreement with the field data. Predominantly constrained to the tideline, microplastics in the model migrate in response to winds during this time. During upwelling-favorable winds, a subset of tracers break from the tideline to travel to the northeast; while during downwelling phases, tracers divert into the plume waters and flush rapidly to the south (Fig. 4). During wind inversions, however, the majority of tracers re-enter the tideline from which tracers feed onto the coast within or near the plume front (Fig. 4). Microplastic concentrations observed in Delaware coastal waters are roughly an order of magnitude lower than those previously observed in the adjacent bay (0.7–3 pieces/m³) (Cohen et al., 2019). Such patterns are characteristic of dilution of particulates during transit from source tributaries to open oceans. For example, in studies of the Chesapeake Bay, a decrease in microplastic concentrations is observed from tributaries to the central bay (Bikker et al., 2020; López et al., 2021), mirroring observed patterns in the Delaware Bay (Cohen et al., 2019). Open ocean concentrations decline further still, with surface concentrations in the north Atlantic ranging from 10^{-3} pieces/m² tens of kilometers offshore to 10^{-1} pieces/m² within major gyres (Kukulka et al., 2012).

While limited, observations of surface larval and microplastic distributions in Delaware and New Jersey coastal waters fall well in line qualitatively with expected particle motions under the recorded wind and river conditions of August 2020. The agreement of field samples with both expected behaviors based on model insight into forcing response and coincident simulations encourages our approach to simulated larval migration patterns and microplastic exposure mechanisms. Moreover, field observations above provide direct evidence for co-occurrence of *C. sapidus* larvae and microplastics at all stations in the
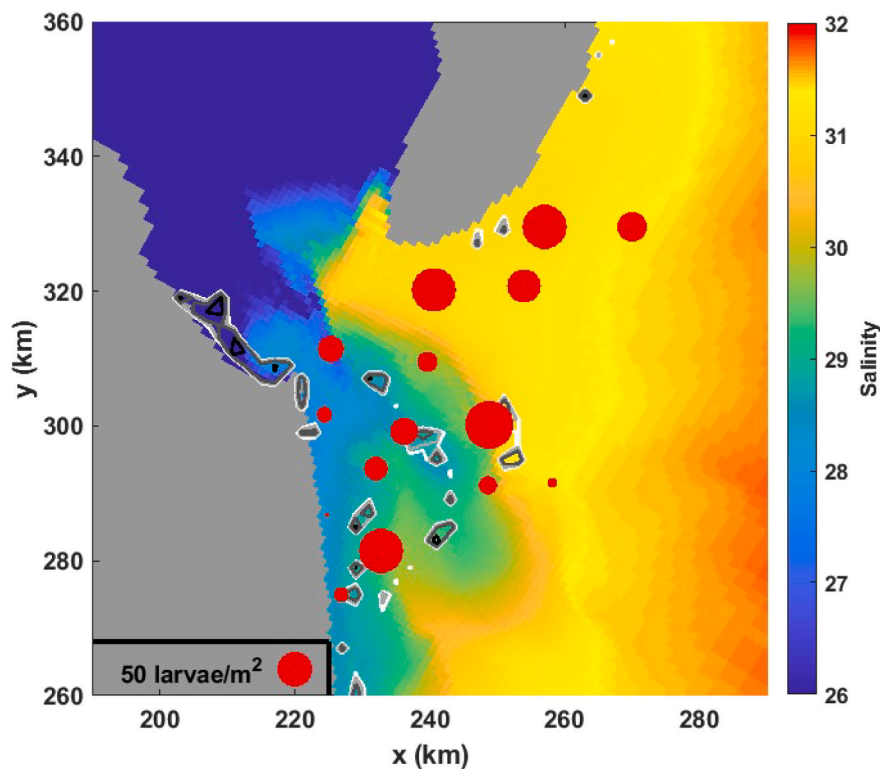

Fig. 5. Observed larval concentrations (red dots scaled by concentrations) in surface waters from August 18–20, 2020 compared to simulated larval distributions (contours) over a representative salinity field. Contour lines are increasingly dark for increasing concentration and represent 1.12 (white), 1.58, 2.51, and 10 (black) larvae/m². (For interpretation of the references to colour in this figure legend, the reader is referred to the web version of this article.)
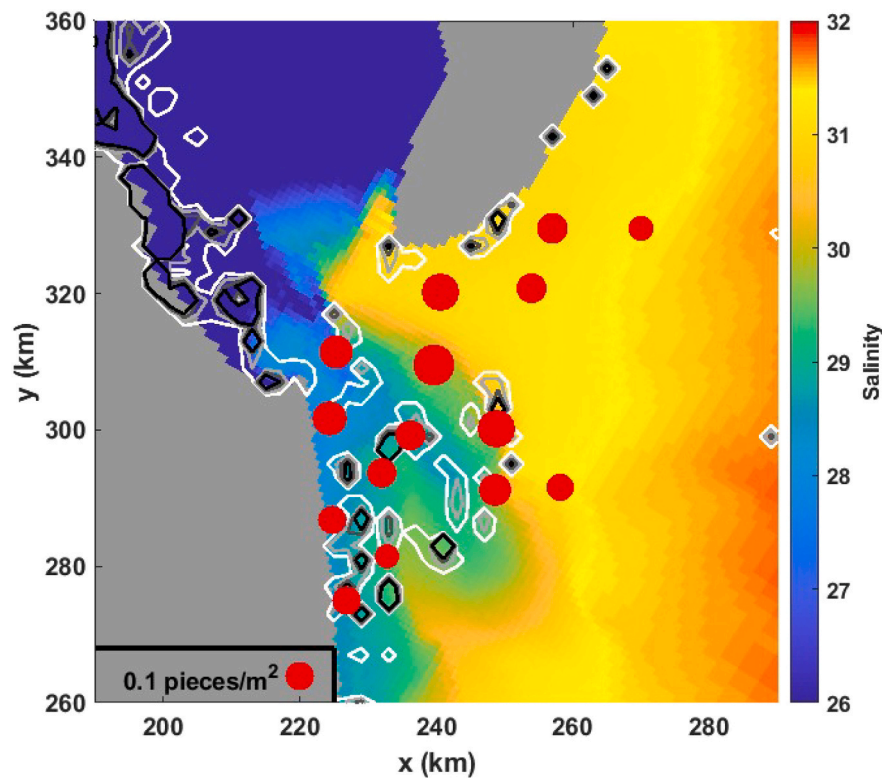
Fig. 6. Observed microplastic concentrations (red dots scaled by concentrations) at 15 sampled stations from August 18–20, 2020 compared to simulated microplastic distributions (contours) over a representative salinity field. Contour lines are increasingly dark for increasing concentration and represent 0.25 (white), 0.75, 1.25, and 1.75 (black) microplastic pieces/m². (For interpretation of the references to colour in this figure legend, the reader is referred to the web version of this article.)

coastal ocean, reinforcing the need to understand the mechanisms and extent of exposure.

3.4. Microplastic exposure pathways

The above sections identify transport pathways and distributions for larvae and microplastics defined by prevailing wind conditions. In this section, we view the tracer paths of larvae and microplastics together in order to summarize the exposure of the *C. sapidus* larvae to this pollutant. Three distinct exposure mechanisms exist in numerical simulations. The first two exposure mechanisms are driven by tracer organization through short-term wind conditions within the bay, while the third mechanism responds to extended wind-driven cross-shelf transport.

3.4.1. In-estuary case 1: tideline-assisted exposure

Intense microplastic exposure can form in the central tideline, commonly overlying the thalweg, under the influence of coastal upwelling-favorable wind fields onset shortly after *C. sapidus* spawning events. In the presence of coastal upwelling-favorable winds, as with microplastic tracers (Fig. 4c), larval tracers migrate north/northeast of the spawning location. Unlike microplastic tracers, which accumulate over the thalweg of the bay during transit to the mouth, larvae are released in the model at the mouth south of plastic-accumulating regions (Fig. 1b). Transport driven by upwelling winds, carries larval tracers towards these plastic-laden waters. Although sustained upwelling winds can displace microplastic tracers to the north (Fig. 4c), the motion is contested by tidally/bathymetrically-induced convergence, which slows such escape. As a result, assuming upwelling-favorable winds onset roughly coincident with larval spawning, larvae are carried into the tideline faster than microplastics can be removed. However, sufficiently sustained upwelling winds prior to larval release can effectively clear the

estuary mouth of microplastic tracers prior to the arrival of larval tracers, mitigating exposure. Frequency of this mechanism can also vary depending upon release location and river discharge, as larval tracers released further from the thalweg and/or under stronger discharge can be flushed from the bay more rapidly than they can be advected to the tideline.

The result of this exposure mechanism is shown in Fig. 7a,b. Rapid relocation of larvae to the tideline before flushing in the riverine outflow brings larval tracers into a distinct microplastic-laden band overlying the thalweg (Fig. 7a). Tideline-assisted exposure can be deemed symptomatic of tidal trapping of larvae, as 62.5 % of larvae within this migration loop first experience high microplastic under early onset northward migration (see Fig. 1b). Amongst all returned larvae, 32.1 % display early exposure related to migration of larvae north into tideline-accumulated microplastics. As a secondary exposure mechanism, particles that follow the buoyant plume loop often spend time near or above the tideline prior to settling at three weeks (Fig. 3).

3.4.2. In-estuary case 2: exposure in the river outflow

While upwelling winds drive exposure if onset is roughly in time with larval release, coastal downwelling-favorable winds generate enhanced exposure when preceding larval releases. Recall from Section 3.2, that downwelling winds transport microplastics from the central tideline into the riverine outflow (Fig. 4b). As a result, although removal from the tideline allows the microplastic to dilute, downwelling winds enhance microplastic concentrations in regions where larvae are released (Fig. 7c). Continued downwelling winds compress larval patches in the coastal current against the coastline, combining with identical behavior in microplastics to generate enhanced microplastic exposure. Exceedingly strong winds (>6 m/s), however, can cause microplastics to rapidly compress along the Delaware coast within the bay, preventing microplastics from reaching the bay mouth, or cause intensification of
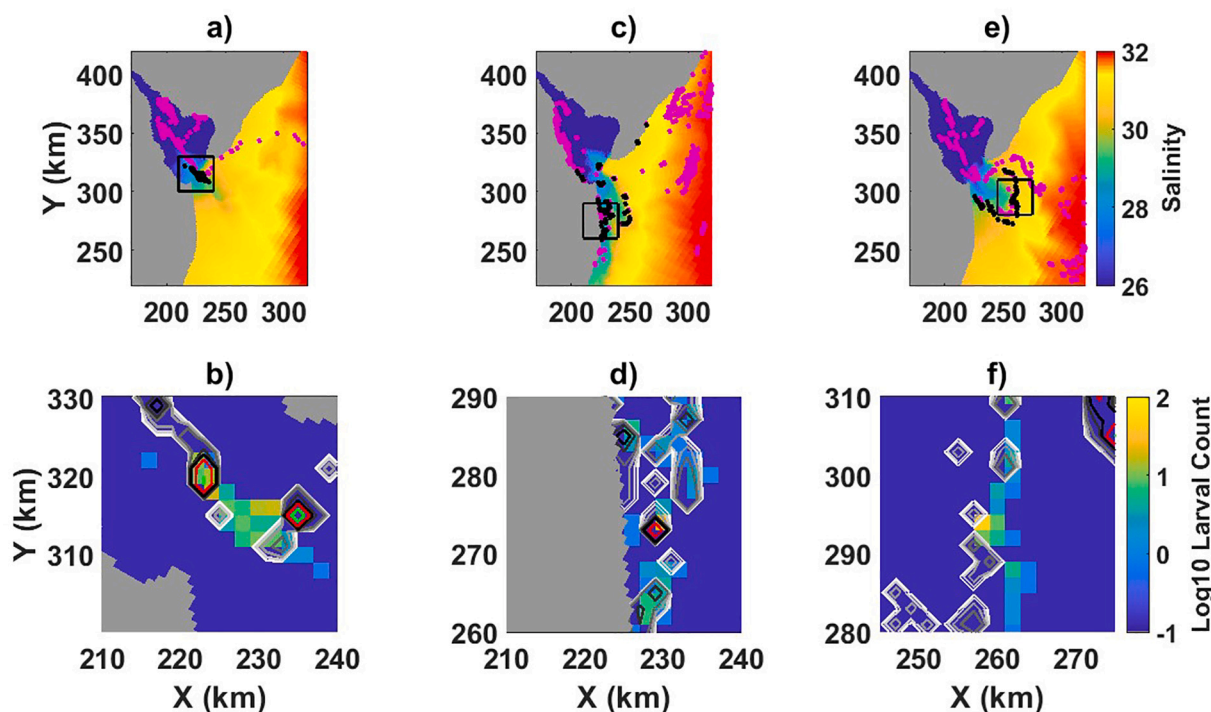
Fig. 7. Sample tracer distributions in (a, b) tideline-assisted microplastic exposure, (c, d) river outflow exposure, and (e, f) offshore frontal exposure, visualized in two formats. (a, c, e) *Callinectes sapidus* (black) and microplastic (magenta) tracers overlying the corresponding background salinity field. (b, d, f) Comparison of larval (background) and microplastic (contours) concentration fields. *C. sapidus* larvae and microplastics are scaled as described in Section 2.2. Grey-tone contour lines represent, in increasing darkness, 0.1, 0.25, 0.5, 1, 3, 6 microplastic pieces/m², while red and green contours represent 15 and 30 pieces/m². (For interpretation of the references to colour in this figure legend, the reader is referred to the web version of this article.)

the coastal current (Fong and Geyer, 2001; Whitney and Garvine, 2005) that flushes microplastics from the bay mouth prior to larval spawning, limiting opportunity for larval exposure.

The critical overlap of downwelling wind dependence links the river outflow exposure to the buoyant plume loop, driving exposure in 88.5 % of larvae that follow this path. Overall, this mechanism is the initial means of exposure in 58.3 % of returned larvae in 2020, nearly twice as frequent as the tideline-assisted exposure. While upwelling and downwelling winds occur with roughly equal frequency, this trend towards outflow exposure likely results from a combination of effective clearing of microplastics from tidelines by upwelling winds and reduced rates of return to the bay in June and July (Tilburg et al., 2005), months dominated by near-constant southwesterly winds (Fig. 2b) that drive particles beyond the plume front. Compression along coastlines are observed to drive microplastic concentrations weaker than those formed in tidelines, which can be seen in Fig. 7b and d through the absence of the red 30 microplastic pieces/m² contour in the latter.

3.4.3. Shelf waters: delayed frontal exposure

The final pathway, offshore frontal exposure, often occurs roughly one to four weeks after larval tracer release, rather than within hours to a couple days in the above mechanisms. This mechanism can occur whenever both larvae and microplastics flush from the bay. On the shelf, along-shelf winds dominantly force cross-shelf flow via Ekman transport (Lentz and Fewings, 2012). Upwelling winds force tracers distributed within the coastal current into concentrated bands within the plume front (Tilburg et al., 2009) (Fig. 7e), leading to aggregation of microplastics and exposure of larvae. However, should one tracer arrive a few days ahead of the other, slow transport across the front (Thomson et al., 2014) can remove either tracer from the system. In such cases, reversal to downwelling-favorable winds can reverse transport and generate an analogous frontal exposure.

The strength of the upwelling winds will play a key role in

determining the efficiency of this mechanism. Just as downwelling winds compress the coastal current against the coastline, upwelling winds spread the coastal current away from the coast, driving shoaling of the plume (Fong and Geyer, 2001; Whitney and Garvine, 2005). Shoaling of the plume relates to enhanced mixing and entrainment of ocean waters, as well as a weaker plume front (Fong and Geyer, 2001; Mazzini and Chant, 2016; Whitney and Garvine, 2005). As such, not only do tracers need to be carried further to reach the plume front, they will more readily cross the front, weakening exposure.

Frontal exposure is the initial exposure source in only 8.8 % of returned larvae, making it the least common form of initial exposure. However, as 85 % of particles follow the offshore wind loop, which consistently involves transport to and temporary residence in the offshore plume front, frontal exposure acts instead as a secondary exposure mechanism following tideline-assisted and river outflow exposure. In response to dilution of the tracer clouds outside the bay (Fig. 4) and an inefficient collection method, plume fronts show lower concentrations of microplastics than do the prior examples, as seen in comparing the contours of Fig. 7b, d, and f.

3.4.4. Mean microplastic exposures

Exposure estimates for returned larvae can be determined from scaled microplastic concentration fields and Lagrangian larval paths (Section 2.2). As expected from the highly variable larval transport paths (Fig. 3) and wind-dependent microplastic distributions (Fig. 4), instantaneous exposure time series are characterized by significant differences from particle to particle, as well as rapid variation in time due to localized, short-lived convergent and divergent flow fields in these complicated coastal systems (Fig. 8a). Mean instantaneous exposures of 2.9 microplastic pieces/m² are comparable to microplastic concentrations of 2.5 pieces/m² near in-bay source tributaries (Cohen et al., 2019), and significantly higher than observed shelf concentrations at the selected 2020 stations (Fig. 6). Overall, 99.1 % of returned larvae in this
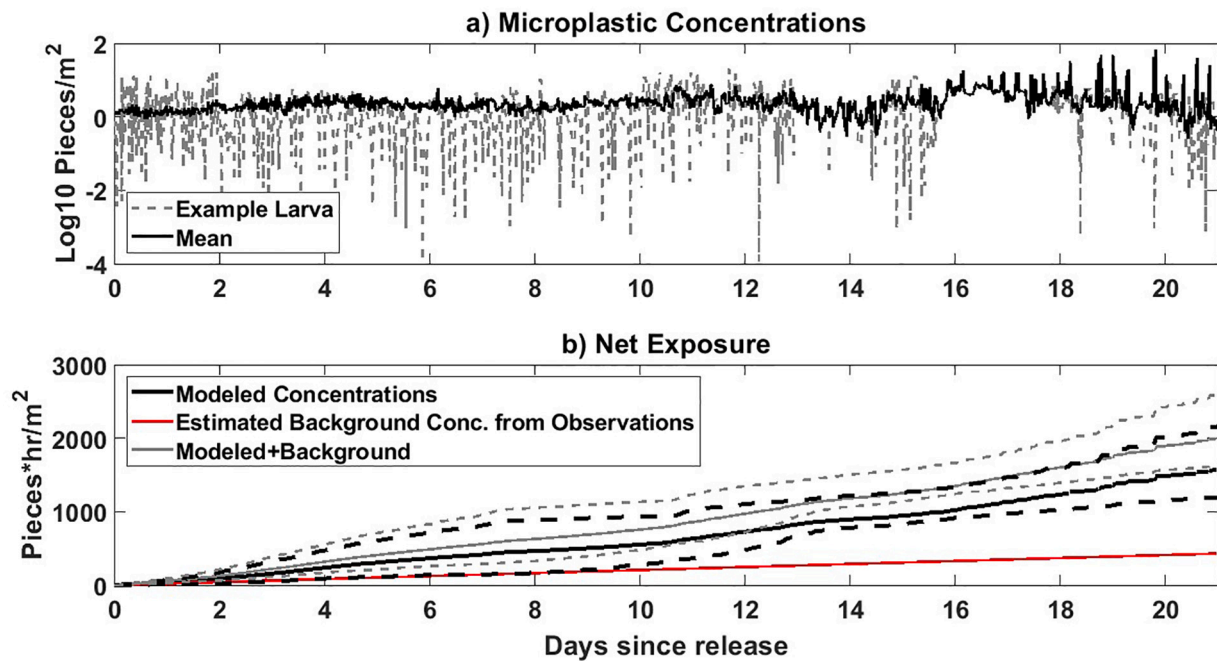
a) Microplastic Concentrations

Fig. 8. (a) Instantaneous exposure time series for a single larval tracer and a mean time series for all larval tracers returned to the bay. (b) Net microplastic exposure time series for modeled larvae. A conservative background exposure estimate is provided by taking the lowest microplastic concentration observed during field sampling and holding this exposure level constant for three weeks. Model results are presented both without (black) and with (grey) background microplastic exposure estimates. Mean net exposures for all returned larvae (solid line) and individual net exposure series for the larvae with greatest and least exposure three weeks following release (dashed) are presented.

simulated 2020 spawning season experience an instantaneous microplastic concentration over 4 pieces/m² at least once during their larval transport, demonstrating clear coupling of larval migration to the above microplastic exposure mechanisms. In viewing a mean time series of instantaneous concentrations, we can identify a few key events defining exposure (Fig. 8a). At the beginning of the time series, exposure is highly variable, depending both upon conditioning of microplastic distribution prior to larval release, as well as early onset wind to direct larval migration post-spawning. Sharp increases of mean exposure occur following days 2 and 8 following release, coinciding with larvae reaching coastlines and tidelines, respectively. Lower exposure concentrations within plume fronts and highly variable delivery times due to plume migration (Fong and Geyer, 2001; Whitney and Garvine, 2005), prevent a comparable signal for frontal exposure. After two weeks, however, the greatest peaks in average instantaneous exposure begin to form, reflecting a return of larvae to the estuary prior to the onset of settlement at three weeks (Tilburg et al., 2005) and consequent collection of particles from the varied larval migration loops near the central tideline.

As with instantaneous exposures, the net exposure experienced prior to settling varies widely between larvae (Fig. 8b). When comparing individual larvae, net exposure at three weeks can differ by a factor of two and with greater disparities occurring over the three weeks (Fig. 8b, dashed lines). High and low exposure larvae highlight exposure timing as a key factor. Larvae exposed to high microplastic concentrations within a couple days following spawning, such as through outflow exposure via preemptive downwelling winds, travel with microplastics throughout their larval lifespans, accumulating net exposure rapidly. Low exposures are observed when larvae must transit to exposure mechanisms, such as tidelines and offshore fronts. When comparing the larva with the lowest individual net exposure (Fig. 8b, lower dashed line) to background observed microplastics levels (red line, derived from the lowest sampled microplastic concentrations), the importance of coupling of larval migration to the above exposure mechanisms can be truly appreciated. A clear exposure event can be observed occurring

between days 10 and 13, as the net exposure sharply increases; Moreover, at three weeks, the net exposure for the larva has been increased by a factor of 3.8, compared to an increase of 4.6× for the mean net exposure. Results indicate clear and consistent encounters between returned larvae and microplastic debris, with marked exposure events visible throughout the varied exposure time series as anticipated from the existence of the distinct exposure mechanisms described above.

3.5. Anticipated impacts of zooplankton-microplastic exposure

Strong aggregation and joint transport of zooplankton and microplastics in the model supports concerns of microplastic exposure amongst surface-concentrated organisms like early-stage *C. sapidus* larvae. Most notably, this organization provides greater opportunity for ingestion of microplastics through amplifying concentrations near zooplankton (Fig. 8). As such ingestion has been previously observed in conjunction with resulting harm to organism health (Cohen et al., 2019; Cole et al., 2013; Gambardella et al., 2017; Sun et al., 2017), these results suggest that regional convergent flow features could exacerbate harm to surface-migrating plankton from buoyant pollutants, including microplastics. In the case of microplastics, the concentrations observed and simulated here (Fig. 6) and the corresponding exposure levels (Fig. 8) still comprise an overall small amount of material per unit volume of seawater. As such, leaching chemicals and any related harm (Talsness et al., 2009) to zooplankton would likely be best considered in regards to ingestion rather than degradation in the environment.

Finally, we consider the role of less buoyant microplastics which mix vertically in the water column. Vertically-mixing tracers undergo a qualitatively similar path to their surface-trapped counterparts, with the majority of returned tracers transporting away from shore before returning with downwelling wind pulses (not pictured). The primary difference between the two cases is the scale of motion. Vertically-mixing tracers undertake a slower mean transport than do surface-trapped tracers. Resulting transport loops, therefore, are constrained much nearer to the mouth of Delaware Bay. Two main consequences

could be possible here, depending on zooplankton interaction with microplastic debris. First, if a portion of microplastic debris is considered as vertically-mixing, a spatial discrepancy will occur relative to surface-advected zooplankton during coastal transit, reducing exposure. Alternatively, some microorganisms have been observed attaching to and riding plastic debris in the oceans (Barnes and Milner, 2005; Zettler et al., 2013). While the extent of this phenomenon is poorly understood, association of zooplankton with vertically-mixing microplastics could enhance retention near estuaries, increasing mean exposure (Cohen et al., 2019; Kukulka and Brunner, 2015) or aiding with migration loops (i.e. - inhibiting cross-shelf loss of larvae).

4. Conclusions

This study utilized a regional model of the Delaware Bay and surrounding coastal ocean built in the Regional Ocean Modeling System (ROMS) framework and a corresponding Lagrangian particle tracking code to assess the exposure mechanisms and exposure levels of coastal zooplankton to emerging microplastic pollutants previously catalogued in the Delaware Bay (Cohen et al., 2019), using the commercially important Atlantic blue crab *Callinectes sapidus* as a sample species. The work presented here focuses on model runs using realistic winds, freshwater discharge, and tides for the 2020 spawning season, backed by field observations of offshore microplastic distributions collected from August 18–20, 2020; although comparable results can be reported for the years 2008–2010. Simulated surface-riding passive tracers were released at locations near the Delaware River and St. Jones/Murderkill River tributaries representing microplastic inputs (Cohen et al., 2019), as well as within the riverine-influenced outflow on the Delaware-side of the bay mouth to represent larval spawning events (Tilburg et al., 2005). Larvae were tracked for three to five weeks post-release as larvae return to the estuary.

Zooplankton tracks confirmed the existence of three major migration pathways reported by Tilburg et al. (2005), while microplastics follow three main distributions based upon wind conditions. Under quiescent winds that do not favor coastal upwelling or downwelling, microplastics arrange in a central tideline over the thalweg of the bay (Cohen et al., 2019; Mason et al., 2022), most likely via tidally-driven convergence (Kukulka and Chant, 2022; Mason et al., 2022; Nunes and Simpson, 1985). Particles tend to leave the bay near the plume front. Under upwelling winds, microplastics deflect towards the New Jersey side of the bay, arranging over shallower channels and flushing from the bay to the northeast. Downwelling winds displace particles into the Delaware River outflow and cause particles to flush rapidly to the south within the coastal current.

Each zooplankton migration pathway links best to one of three microplastic exposure mechanisms. Tidal-trapping occurs when upwelling winds transport zooplankton to or above the thalweg, creating intense exposure in microplastic patches formed via tidelines. The buoyant plume loop coincides with displacement of microplastics into the riverine outflow and enhanced exposure along the coast due to compression of the coastal current and particle patches (Whitney and Garvine, 2005). The offshore wind loop collects microplastics and zooplankton tracers at the offshore plume front in coastal waters, generating enhanced exposures. For returned larvae, high microplastic exposure is nearly universal. The net microplastic exposure experienced by larvae is heavily tied to early and preceding wind conditions and zooplankton migration path; however, net exposure averages $4.6\times$ greater at three weeks for returned larvae compared to conservatively estimated minimum levels derived from field observations as a result of microplastic and zooplankton aggregation.

Despite multiple distinct zooplankton migration pathways and equally distinct coastal arrangements of microplastics, coincident transport of these particles nonetheless brings the two into contact with an overall frequency of 99.1 %. *C. sapidus* larval migrations impose a tendency for larvae to collect in regional convergent flow structures (estuarine tidelines and plume fronts) that collect microplastics. While the predominant complex offshore larval migration of *Callinectes sapidus* has the unexpected benefit of limiting microplastic exposure compared to life within the bay, high microplastic exposure levels in response to preliminary concentration of microplastics within the Delaware Bay, distribution of larvae and microplastics within coastal oceans via surface winds, and collection and organization of larvae and microplastics via plume fronts drives potentially concerning levels of microplastic exposure for these crucial recruits to the fishery.

CRediT authorship contribution statement

Todd X. Thoman: Conceptualization, Methodology, Investigation, Writing – original draft. **Tobias Kukulka:** Conceptualization, Methodology, Writing – review & editing, Supervision, Funding acquisition. **Jonathan H. Cohen:** Conceptualization, Writing – review & editing, Funding acquisition. **Hayden Boettcher:** Investigation, Writing – review & editing.

Declaration of competing interest

The authors declare that they have no known competing financial interests or personal relationships that could have appeared to influence the work reported in this paper.

Data availability

Data will be made available on request.

Acknowledgments

References

Barnes, D., Milner, P., 2005. Drifting plastic and its consequences for sessile organism dispersal in the Atlantic Ocean. Mar. Biol. 146, 815–825. https://doi.org/10.1007/s00227-004-1474-8.

Biermann, J., North, E., Boicourt, W., 2016. The distribution of blue crab (*Callinectes sapidus*) megalopae at the mouths of Chesapeake and Delaware Bays: implications for larval ingress. Estuar. Coasts 39, 201–217. https://doi.org/10.1007/s12237-015-9978-7.

Bikker, J., Lawson, J., Wilson, S., Rochman, C., 2020. Microplastics and other anthropogenic particles in the surface waters of the Chesapeake Bay. Mar. Pollut. Bull. 156 (111257) https://doi.org/10.1016/j.marpolbul.2020.111257.

Bullard, S., 2003. Larvae of Anomuran and Brachyuran Crabs of North Carolina. Crustaceana Monographs, 1. Brill, Leiden. https://doi.org/10.1163/9789004475908.

Castellano, P., Kirby, J., 2011. Validation of a Hydrodynamic Model of Delaware Bay and the Adjacent Caostal Region. (Res. Rept. CACR-11-03). Center for Applied Coastal Research, University of Delaware, Newark, DE.

Cohen, J., Internicola, A., Mason, R., Kukulka, T., 2019. Observations and simulations of microplastic debris in a tide, wind, and freshwater-driven estuarine environment: the Delaware Bay. Environ. Sci. Technol. 53 (24), 14204–14211. https://doi.org/10.1021/acs.est.9b04814.

Cole, M., Lindeque, P., Fileman, E., Halsband, C., Goodhead, R., Moger, J., Galloway, T., 2013. Microplastic ingestion by zooplankton. Environ. Sci. Technol. 47 (12), 6646–6655. https://doi.org/10.1021/es400663f.

Cole, M., Lindeque, P., Fileman, E., Halsband, C., Galloway, T., 2015. The impact of polystyrene microplastics on feeding, function, and fecundity in the marin copepod *Calanus helgolandicus*. Environ. Sci. Technol. 49 (2), 1130–1137. https://doi.org/10.1021/es504525u.

Costlow Jr., J., Bookhout, C., 1959. The larval development of *Callinectes sapidus* Rathbun reared in the laboratory. Biol. Bull. 116 (3), 373–396. https://doi.org/10.2307/1538947.

Dittel, A., Epifanio, C., 1982. Seasonal abundance and vertical distribution of crab larvae in Delaware Bay. Estuaries 5 (3), 197–202. https://doi.org/10.2307/1351835.

Epifanio, C., 2019. Early life history of the blue crab *Callinectes sapidus*: a review. J. Shellfish Res. 38 (1), 1–22. https://doi.org/10.2983/035.038.0101.

Epifanio, C., Cohen, J., 2016. Behavioral adaptations in larvae of brachyuran crabs: a review. J. Exp. Mar. Biol. Ecol. 482, 85–105. https://doi.org/10.1016/j.jembe.2016.05.006.

Epifanio, C., Garvine, R., 2001. Larval transport on the Atlantic continental shelf of North America: a review. Estuar. Coast. Shelf Sci. 52, 51–77. https://doi.org/10.1006/ecss.2000.0727.

Fong, D., Geyer, W., 2001. Response of a river plume during an upwelling favorable wind event. J. Geophys. Res. 106 (C1), 1067–1084.

Gambardella, C., Morgana, S., Ferrando, S., Bramini, M., Piazza, V., Costa, E., Garavena, F., Faimali, M., 2017. Effects of polystyrene microbeads in marine planktonic crustaceans. Ecotoxicol. Environ. Saf. 145, 250–257. https://doi.org/10.1016/j.ecoenv.2017.07.036.

Hale, R., Seeley, M., La Guardia, M., Mai, L., Zeng, E., 2020. A global perspective on microplastics. J. Geophys. Res. 125, e2018JC014719 https://doi.org/10.1029/2018JC014719.

Jivoff, P., Smith, J., Sodi, V., Van Morter, S., Faugno, K., Werda, A., Shaw, M., 2017. Population structure of adult blue crabs, *Callinectes sapidus*, in relation to physical characteristics in Barnegat Bay, New Jersey. Estuar. Coasts 40, 235–250. https://doi.org/10.1007/s12237-016-0127-8.

Kukulka, T., Brunner, K., 2015. Passive buoyant tracers in the ocean surface boundary layer: 1. Influence of equilibrium wind-waves on vertical distributions. J. Geophys. Res. Oceans 120 (5), 3837–3858. https://doi.org/10.1002/2014JC010487.

Kukulka, T., Chant, R., 2022. Surface convergence zones due to lagrangian residual flow in tidally driven estuaries. J. Phys. Oceanogr. https://doi.org/10.1175/JPO-D-22-0067.1.

Kukulka, T., Proskurowski, G., Morét-Ferguson, S., Meyer, D.W., Law, K.L., 2012. The effect of wind mixing on the vertical distribution of buoyant plastic debris. Geophys. Res. Lett. 39 (L07601) https://doi.org/10.1029/2012GL051116.

Kukulka, T., Jenkins III, R., Kirby, J., Shi, F., Scarborough, R., 2017. Surface wave dynamics in Delaware Bay and its adjacent coastal shelf. J. Geophys. Res. 122, 8683–8706. https://doi.org/10.1002/2017JC013370.

Lentz, S., Fewings, M., 2012. The wind- and wave-driven inner-shelf circulation. Annu. Rev. Mar. Sci. 4, 317–343. https://doi.org/10.1146/annurev-marine-120709-142745.

López, A., Najjar, R., Friedrichs, M., Hickner, M., Wardrop, D., 2021. Estuaries as filters for riverine microplastics: simulations in a large, coastal-plain estuary. Front. Mar. Sci. 8, 715924. https://doi.org/10.3389/fmars.2021.715924.

Mason, R., Kukulka, T., Cohen, J., 2022. Effects of particle buoyancy, release location, and diel vertical migration on exposure of marine organisms to microplastics in Delaware Bay. Estuar. Coast. Shelf Sci. 275 (107990) https://doi.org/10.1016/j.ecss.2022.107990.

Mazzini, P., Chant, R., 2016. Two-dimensional circulation and mixing in the far field of a surface-advected river plume. J. Geophys. Res. 121, 3757–3776. https://doi.org/10.1001/2015JC011059.

McConaugha, J., Johnson, D., Provenzano, A., Maris, R., 1983. Seasonal distribution of larvae of *Callinectes sapidus* (Crustacea: Decapoda) in the waters adjacent to Chesapeake Bay. J. Crustac. Biol. 3 (4), 582–591. https://doi.org/10.2307/1547953.

Natunewicz, C., Epifanio, C., 2001. Spatial and temporal scales of patches of crab larvae in coastal waters. Mar. Ecol. Prog. Ser. 212, 217–222. https://doi.org/10.3354/meps212217.

Nunes, R., Simpson, J., 1985. Axial convergence in a well-mixed estuary. Estuar. Coast. Shelf Sci. 20 (5), 637–649. https://doi.org/10.1016/0272-7714(85)90112-X.

Ogburn, M., Habegger, L., 2015. Reproductive status of *Callinectes sapidus* as an indicator of spawning habitat in the South Atlantic Bight, USA. Estuar. Coasts 38, 2059–2069. https://doi.org/10.1007/s12237-015-9962-2.

Provenzano Jr., A., McConaugha, J., Philips, K., Johnson, D., Clark, J., 1983. Vertical distribution of first stage larvae of the blue crab, *Callinectes sapidus*, at the mouth of Chesapeake Bay. Estuar. Coast. Shelf Sci. 16 (5), 489–499. https://doi.org/10.1016/0272-7714(83)90081-1.

Quinn, B., Murphy, F., Ewins, C., 2017. Validation of density separation for the rapid recovery of microplastics from sediment. Anal. Methods 9, 1491–1498. https://doi.org/10.1039/C6AY02542K.

Rochman, C., Tahir, A., Williams, S., Baxa, D., Lam, R., Miller, J., Teh, F., Werorilangi, S., Teh, S., 2015. Anthropogenic debris in seafood: plastic debris and fibers from textiles in fish and bivalves sold for human consumption. Sci. Rep. 5 (14340) https://doi.org/10.1038/srep14340.

Sandifer, P., 1972. Morphology and Ecology of Chesapeake Bay Decapod Crustacean Larvae (Ph.D. thesis). The College of William & Mary. https://doi.org/10.21220/nvqc-dn53.

Setälä, O., Fleming-Lehtinen, V., Lehtiniemi, M., 2014. Ingestion and transfer of microplastics in the planktonic food web. Environ. Pollut. 185, 77–83. https://doi.org/10.1016/j.envpol.2013.10.013.

Shchepetkin, A., McWilliams, J., 2005. The regional oceanic modeling system (ROMS): a split-explicit, free-surface, topography-following-coordinate oceanic model. Ocean Model 9 (4), 347–404. https://doi.org/10.1016/j.ocemod.2004.08.002.

Song, Y., Haidvogel, D., 1994. A semi-implicit ocean circulation model using a generalized topography-following coordinate system. J. Comp. Phys. 115 (1), 228–244. https://doi.org/10.1006/jcph.1994.1189.

Sun, X., Li, Q., Zhu, M., Liang, J., Zheng, S., Zhao, Y., 2017. Ingestion of microplastics by natural zooplankton groups in the northern South China Sea. Mar. Pollut. Bull. 115 (1–2), 217–224. https://doi.org/10.1016/j.marpolbul.2016.12.004.

Talsness, C., Andrade, A., Kuriyama, S., Taylor, J., vom Saal, F., 2009. Components of plastic: experimental studies inanimals and relevance for human health. Philos. Trans. R. Soc. B 364, 2079–2096. https://doi.org/10.1098/rstb.2008.0281.

Tankersley, R., Wieber, M., Sigala, M., Kachurak, K., 1998. Migratory behavior of ovigerous blue crabs *Callinectes sapidus* - evidence for selective tidal-stream transport. Biol. Bull. 195 (2), 168–173. https://doi.org/10.2307/1542824.

Thomson, J., Horner-Devine, A., Zippel, S., Rusch, C., Geyer, W., 2014. Wave breaking turbulence at the offshore front of the columbia river plume. Geophys. Res. Lett. 41, 8987–8993. https://doi.org/10.1002/2014GL062274.

Tilburg, C., Whitney, M., Reager, J., 2005. The physics of blue crab larval recruitment in Delaware Bay: a model study. J. Mar. Res. 63, 471–495.

Tilburg, C., Dittel, A., Epifanio, C., 2009. High concentrations of blue crab (*Callinectes sapidus*) larvae along the offshore edge of a coastal current: effects of convergent circulation. Fish. Oceanogr. 18 (3), 135–146. https://doi.org/10.1111/j.1365-2419.2009.00502.x.

Whitney, M., Garvine, R., 2005. Wind influence on a coastal buoyant outflow. J. Geophys. Res. 110 (C03014) https://doi.org/10.1029/2003JC002261.

Whitney, M., Garvine, R., 2006. Simulating the delaware bay buoyant outflow: comparison with observations. J. Phys. Oceanogr. 36 (1), 3–21. https://doi.org/10.1175/JPO2805.1.

Zettler, E., Mincer, T., Amaral-Zettler, L., 2013. Life in the "plastisphere": microbial communities on plastic marine debris. Environ. Sci. Technol. 47, 7137–7146. https://doi.org/10.1021/es401288x.